Materials Express

Copyright © 2015 by American Scientific Publishers
All rights reserved.
Printed in the United States of America

2158-5849/2015/5/001/007
doi:10.1166/mex.2015.1227
www.aspbs.com/mex

Magnesium doped ZnO nanostructures synthesis using *citrus aurantifolia* extracts: Structural and field electron emission properties

Hartini Ahmad Rafaie[1,2,*], Roslan Md. Nor[1,*], and Yusoff Mohd Amin[1]

[1]*Department of Physics, Faculty of Sciences, University of Malaya, 50603 Kuala Lumpur, Malaysia*
[2]*Faculty of Applied Sciences, Universiti Teknologi MARA (UiTM), 40450 Shah Alam, Selangor, Malaysia*

ABSTRACT

We report here the field electron emission performance of pure ZnO and Mg doped ZnO nanostructures prepared on aluminium substrates using *Citrus Aurantifolia* by the sol–gel method. XRD analysis confirmed that the pure ZnO and Mg-doped ZnO nanostructures were polycrystalline with the hexagonal wurtzite crystal structure. Based on EDX analysis, the Mg atomic percentage incorporated in the ZnO samples increased with increasing Mg concentration during synthesis. With Mg doping, the field electron emission performance was significantly affected possibly due to increase in electrical conductivity with doping level. The turn-on electric field values for ZnO nanostructures decreased as dopant concentration increased with values of 6.99, 6.35, 6.07 and 5.99 V/μm for pure ZnO, and 3, 5, and 10 mol% Mg-doped ZnO nanostructures respectively. Almost similar trend was observed for the threshold electric field values of 9.16, 9.17, 8.62 and 8.49 V/μm for pure ZnO, and 3, 5, and 10 mol% Mg-doped ZnO nanostructures, respectively. Field enhancement factor, β, showed no significant trend and was comparable for all samples mainly due to the similar geometrical features of the samples. Emission currents up to a few mAs and with good stability obtained with Mg doping are potentially applicable in field emission technology.

Keywords: ZnO, *Citrus Aurantifolia*, Sol–gel, Structural, Field Electron Emission.

Article

1. INTRODUCTION

ZnO is a direct band gap semiconductor (wide bandgap of 3.37 eV) with a large exciton binding energy of 60 meV.[1] It has attracted interest due to its useful characteristics such as non-toxicity, cheap, relatively high abundance, biocompatible and chemically stable.[2–4] There are several methods for the growth of ZnO nanostructures. However, the most energy-efficient and economical method for synthesizing ZnO nanostructures is the sol–gel method. The sol–gel method has attracted attention as it is a relatively low cost process and represents an ideal method for growing ZnO nanostructures for use in applications such as sensors,[5] solar cells,[6] field emission application,[7–9] optoelectronic, catalysis, and biomedical devices.

In recent years, there has been an increasing interest in green nanotechnology which utilizes biomaterial as a source for the synthesis of nanomaterials. This is an eco-friendly alternative to minimize or totally eliminate hazardous chemicals commonly used for nanomaterials synthesis. Many researchers have reported the formation of gold and silver nanoparticles using biomaterial sources such as micro-organism, yeast, and plant due to the more efficient, inexpensive, eco-friendly and non-toxic approach.[10–12] ZnO nanoparticles are also previously synthesized using biomaterials such as Aloe vera leaf extract,[13] milky latex of *Calotropisprocer* [14] and *Citrus aurantifolia* extract.[15]

*Authors to whom correspondence should be addressed.
Emails: tinie5636@gmail.com, rmdnor@um.edu.my

Article

In this study, we synthesized ZnO nanostructures using *C. Aurantifolia* as a reducing agent and adding a different concentration of Magnesium (Mg) as a dopant by sol–gel method. *C. Aurantifolia* also known as lime is one of the familiar fruit in the citrus fruit family (Rutaceae). Mg was selected as the dopant element for the similarity in Zn^{2+} and Mg^{2+} ionic radii, which make doping plausible. It has been reported that modulation of band gap and UV luminescence intensity resulted from Mg doping.[16]

To the best of our knowledge, there has been no previous report on the synthesis of Mg-doped ZnO nanostructures by using *C. Aurantifolia* extract. The product synthesized in the present technique is comparable to those obtained from conventional reducing agents such as hexamethylenetetramine (HMTA) or cetyltrimethylammonium bromide (CTAB). In this study, pure and Mg-doped ZnO nanostructures were then characterized using Field Emission Scanning Electron Microscope (FESEM), Energy Dispersive X-ray (EDX), X-ray diffraction (XRD) and tested for Field Electron Emission (FEE) application.

2. EXPERIMENTAL PROCEDURE

2.1. Preparation of *C. Aurantifolia* Extract

250 g *C. Aurantifolia* fruits were peeled and the fruit pulp was blended with 250 ml DI water. The blended slurry was filtered using muslin cloth to remove large particles. The liquid extract obtained was further filtered using a 200 nm pore syringe filter. The final *C. Aurantifolia* extract was stored at 4 °C until further use.

2.2. Synthesis of Mg-doped ZnO

Synthesis of ZnO nanostructures was done using the sol–gel immersion technique. 0.55 g zinc nitrate hexahydrate ($Zn(NO)_3 \cdot 6H_2O$) was dissolved in 50 ml *C. Aurantifolia* extract and 0.1 M sodium hydroxide (NaOH) was added dropwise until the pH of the solution was 11. For the synthesis of Mg doped ZnO, 16.5, 27.5 and 55.04 mg magnesium nitrate hexahydrate ($Mg(NO_3)_2 \cdot 6H_2O$) was added to the stock solutions which corresponded to 3, 5 and 10 mol% Mg with respect to zinc. The solutions were stirred continuously for 2 hours at room temperature and then aged for 24 hours before deposition process. Al substrates were used and were immersed in the stock solutions heated to 90 °C for 3 hours for pure and Mg doped ZnO nanostructure deposition.

Structural characterization was carried out using XRD over the 2θ range of 30–80° using Cu Kα radiation (1.546 Å) with 0.01° step size and at room temperature. FESEM equipped with EDX attachment was utilized to analyze the surface morphology and chemical composition of the ZnO nanostructures. Field electron emission measurements were conducted using the diode configuration at a pressure of 10^{-7} mbar using a Keithley 2410 source meter unit. The distance between the cathode of pure or Mg doped ZnO and a copper anode was 120 μm measured

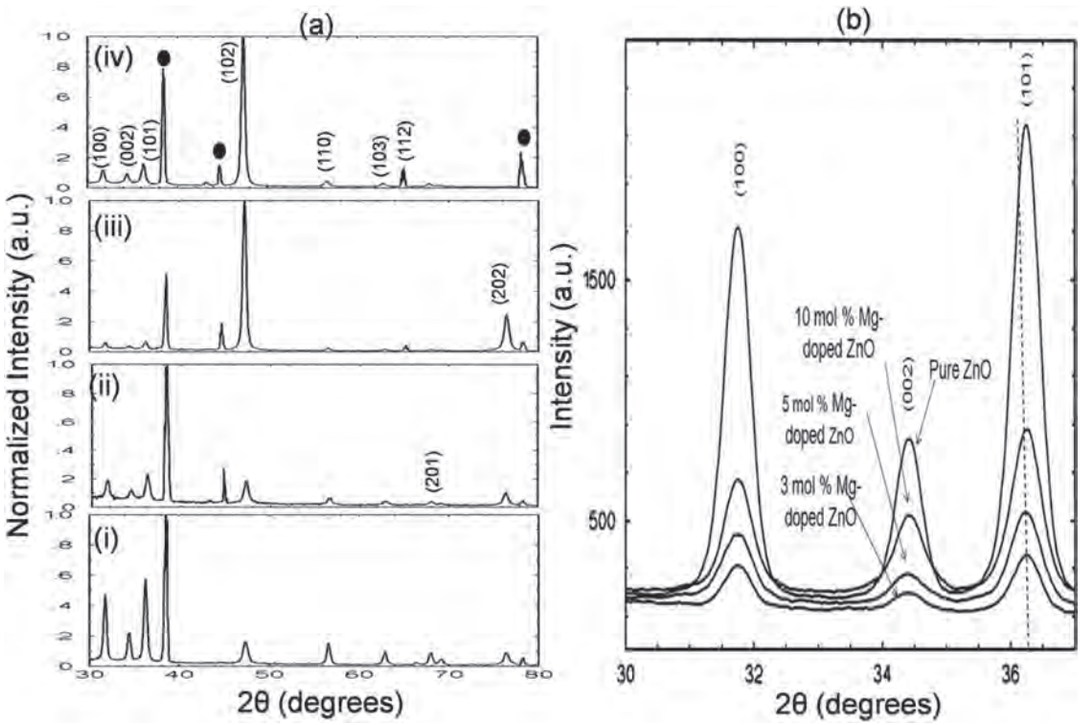

Fig. 1. (a) Normalized XRD patterns of (i) pure ZnO, and (ii) 3, (iii) 5 and (iv) 10 mol% Mg-doped ZnO nanostructures (black circle represent Al peak) and (b) enlarged XRD patterns of pure ZnO, and 3, 5, and 10 mol% Mg-doped ZnO nanostructures in the range 30–37°.

Table I. Peak positions of XRD peaks of pure ZnO and Mg doped ZnO nanostructures compared to standard values.

(hkl) plane (2θ)/Sample	(100)	(002)	(101)	(102)	(110)	(103)	(112)	(201)	(202)
Pure ZnO	31.74	34.37	36.23	47.37	56.68	62.88	67.97	69.13	–
3 mol% Mg-doped ZnO	31.75	34.47	36.25	47.27	56.54	62.90	67.97	69.03	76.28
5 mol% Mg-doped ZnO	31.76	34.38	36.29	47.23	56.64	62.84	68.01	69.13	76.38
10 mol% Mg-doped ZnO	31.82	34.39	36.30	47.30	56.73	62.93	68.02	–	76.39
JCPDS No. 01-079-2205	31.766	34.419	36.251	47.536	56.591	62.852	67.942	69.080	76.953

using a micrometer gauge attached to the anode. The resolution of the micrometer gauge was 10 μm. The effective emission area was 0.25 cm^2. All the measurements were carried out at room temperature.

3. RESULTS AND DISCUSSION

3.1. X-ray Diffraction

Figure 1(a) shows the normalized XRD spectra of pure ZnO and Mg-doped ZnO nanostructures at 3, 5, and 10 mol% Mg doping respectively and the enlarged part of the spectra was shown in Figure 1(b). The XRD pattern exhibit seven major diffraction peaks which can be assigned to (100), (002), (101), (102), (110), (103) and (112) ZnO planes respectively and all the samples exhibit the hexagonal wurzite structure which is in good agreement with JCPDS card No. 01-079-2205. The peak positions are tabulated in Table I.

Also, present are peaks due to the Al substrates at 38.5, 44.7, and 65.1° attributed to diffraction from the Al (111), (200) and (220) faces based on standard values (JCPDS No. 01-085-1327).

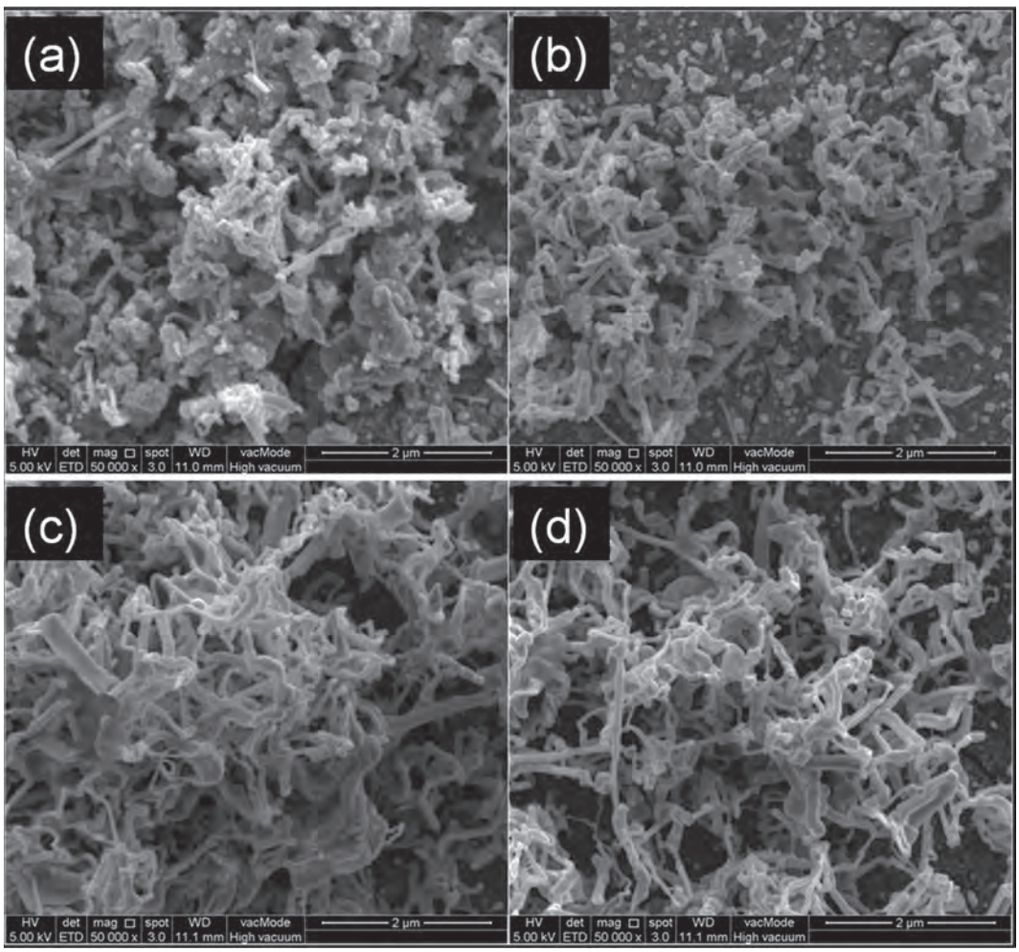

Fig. 2. FESEM images of (a) pure ZnO (b) 3 mol% Mg-doped ZnO, (c) 5 mol% Mg-doped ZnO and (d) 10 mol% Mg-doped ZnO nanostructures.

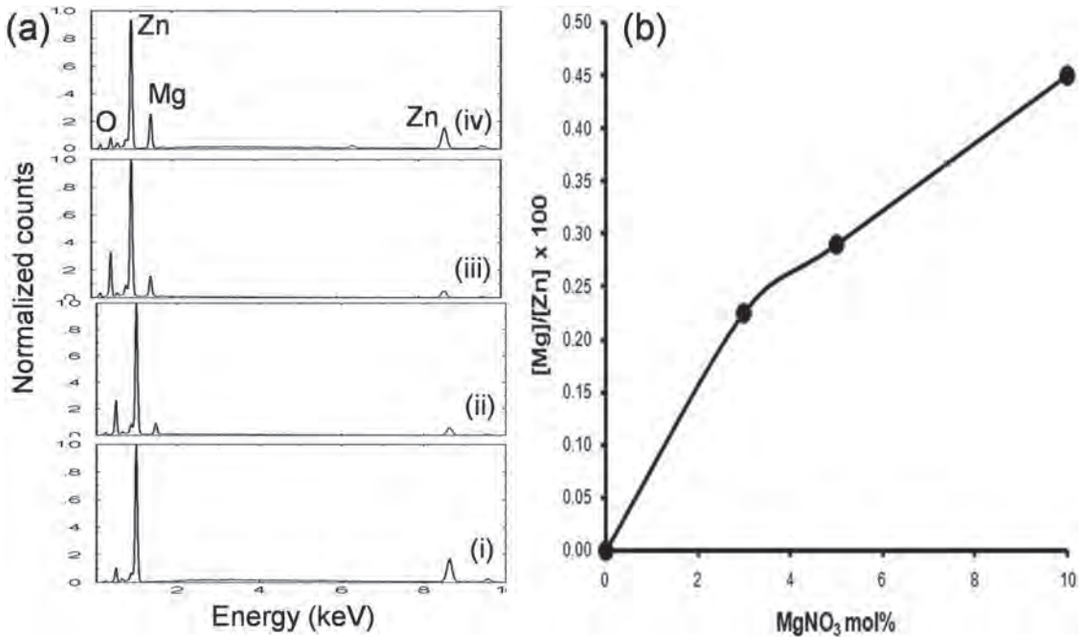

Fig. 3. (a) EDX spectra of (i) pure ZnO (ii) 3 mol% Mg-doped ZnO, (iii) 5 mol% Mg-doped ZnO and (iv) 10 mol% Mg-doped ZnO nanostructures and (b) The Mg atomic percent ratio over Zn from EDX versus $MgNO_3$ (mol%) used during the synthesis.

Figure 1(b), shows the close up view of the (100), (002) and (101) diffraction peaks for all samples. It was found that as the Mg concentration increased, the position of XRD peaks shifted towards higher angle which was evident of Mg doping. The shift in peak positions toward higher angle with increasing Mg doping level was due to the smaller ionic radius of Mg^{2+} compared to Zn^{2+}.[17, 18]

3.2. FESEM and EDX Analysis

Figure 2 shows the surface morphologies of pure ZnO, and 3, 5, and 10 mol% Mg-doped nanostructures. It can be seen that all samples exhibit a fiber-like structure with different aspect ratio. The ZnO nanostructures both pure and Mg doped ZnO were not dense. This feature is favorable for field electron emission applications since dense nanostructures will induce electric field shielding that will impede electron emission. The diameter of ZnO nanostructures was approximately between 20 nm and 150 nm.

The composition of the pure ZnO and Mg-doped ZnO nanostructures is shown in Figures 3(a) and (b). The Mg atomic percent from EDX shows that the amount of Mg in the sample increased with increasing dopant concentration during synthesis at 0.225, 0.29 and 0.45% for 3, 5, and 10 mol% Mg respectively.

3.3. Field Electron Emission (FEE) Measurement

FEE properties of pure ZnO and Mg-doped ZnO nanostructures in the form of emission current density versus the applied electric field (J-E) plots are depicted in Figure 4(a). The results were analyzed based on the Fowler Nordheim equation,[19] given by:

$$J = \left(\frac{A\beta^2 E^2}{\varphi}\right)\exp\left(-\frac{B\varphi^{3/2}}{\beta E}\right) \quad (1)$$

Where J is the current density, the applied field (E) is defined as $E = V/d$, where V is the applied potential and d is the separation between anode and cathode. φ(eV) is the work function of the emitting material, which is 5.3 eV for ZnO,[20] β is the field enhancement factor, while A and B are constant with value $A = 1.56 \times 10^{-6}$ AeV V^{-2} and $B = 6.83 \times 10^9$ $eV^{-3/2}$ Vm^{-1}. Equation (1) is linearized to obtain the FN plot and,

$$\beta = \frac{B\varphi^{3/2}}{m_{\text{slope}}} \quad (2)$$

where m_{slope} is the gradient of the FN plot.

The turn on field and the threshold field, defined as electric fields required to produce 1 μA/cm^2 and 100 μA/cm^2 respectively, were obtained from the J–E curves shown in Figure 4(a). Results from this work are tabulated in Table II, together with previously reported results for comparison.

Apart from threshold on field values for pure and 3 mol% Mg doped samples, our results showed a general trend of decreasing turn on and threshold field values with increasing Mg doping levels. The threshold fields seemed to be almost equal for pure and 3 mol% Mg doped samples at 9.16 and 9.17 V/μm before receding to 8.62 and 8.49 V/μm, for samples doped with 5 and 10 mol% Mg respectively. The turn on field values shows a much clearer

Article

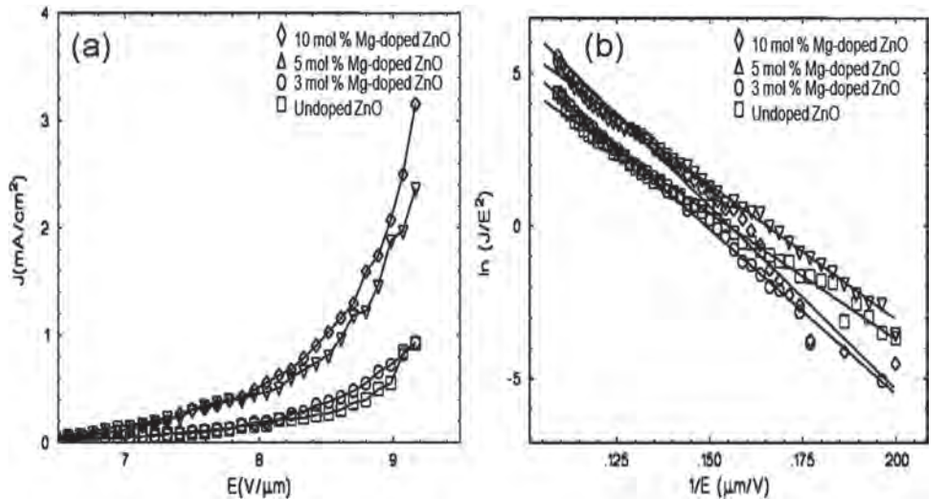

Fig. 4. (a) J–E field emission plot from pure ZnO, 3 mol% Mg-doped ZnO, 5 mol% Mg-doped ZnO, and 10 mol% Mg-doped ZnO nanostructures, (b) the corresponding F–N plot.

trend i.e., 6.99 V/μm was recorded for pure sample compared to 5.99 V/μm for the sample doped with 10 mol% Mg. Based on the present understanding, the two main factors that may affect the turn on and threshold field values are emission cathode geometry and electrical conductivity. Based on FESEM imaging, the structures and geometry of our samples were almost identical. As such, the main reason for the trend observed in the increase in the electrical conductivity of the ZnO nanostructures with increasing doping levels. Such increase in conductivity is evident in the values of the maximum current density measured at 10 V/μm of 0.8, 0.9, 2.4 and 3.2 mA/cm^2 for pure ZnO, 3, 5, and 10 mol% Mg doped samples, respectively (Fig. 4(a)).

The FN plots obtained for all samples are shown in Figure 4(b). For all samples, the FN plots were well fitted to straight lines. The field enhancement factors, β, obtained from the fitted straight line are tabulated in Table II. The β values showed no clear correlation with Mg doping level. This is understandable since β values are predominantly influenced by emitter geometry, for example, emitters with high aspect ratio and sharp tips tend to produce the highest enhancement.[21, 22] This is evident from the results previously reported shown in Table II.

Table II. Field electron emission parameters of pure ZnO and Mg doped ZnO nanostructures.

ZnO nanostructure	Substrate	Turn-on field value for (V/μm)	Threshold field value (V/μm)	Field enhancement factor, β	Reference
Pure ZnO nanofiber	Aluminum	6.99 (1 μA/cm^2)	9.16 (100 μA/cm^2)	801	(This work)
3 mol% Mg-doped ZnO nanofiber		6.35(1 μA/cm^2)	9.17(100 μA/cm^2)	965	
5 mol% Mg-doped ZnO nanofiber		6.07(1 μA/cm^2)	8.62(100 μA/cm^2)	955	
10 mol% Mg-doped ZnO nanofiber		5.99(1 μA/cm^2)	8.49(100 μA/cm^2)	786	
Mg-doped ZnO tetrapods	Powder form	2.6	–	2327	[23]
ZnO nanospikes	ITO glass	3.2 (1 μA/cm^2)	6.6	2364	[24]
Pin-cushion cactus like ZnO nanopencil	Zn foil	1.38 (0.1 μA/cm^2)	2.84 (49 μA/cm^2)	–	[25]
Cu/ZnO Nanocomposite film	Zn foil	1.56	3.12 (0.1 mA/cm^2)	–	[26]
ZnO nanowalls	ITO glass	4.8 (0.1 μA cm^{-2})	–	4700	[27]
ZnMgO/Au (10 nm) nanowires	Si	0.78 (10 mA/cm^2)	1.22 (100 mA/cm^2)	2310	[28]
ZnMgO/Au (30nm) nanowires		1.62 (10 mA/cm^2)	2.32 (100 mA/cm^2)	1140	
ZnO Nanopillars	PET	1.2 (1 μA/cm^2)	–	23104	[29]
ZnO Nanowalls		2.2 (1 μA/cm^2)		5256	
Sn doped ZnO nanowires	Zn foil	0.53 (1 μA/cm^2)	1.1 (100 μA/cm^2)	–	[30]
		1.52 (1 μA/cm^2)	2.25 (100 μA/cm^2)		
ZnO nanowires (0.002 M)	Zn foil	1.24 (1 μA/cm^2)	1.9 (10 μA/cm^2)	–	[31]
ZnO nanowires (0.004 M)		1.2 (1 μA/cm^2)	1.64 (10 μA/cm^2)		
ZnO nanowires (0.016 M)		1.32 (1 μA/cm^2)	1.96 (10 μA/cm^2)		

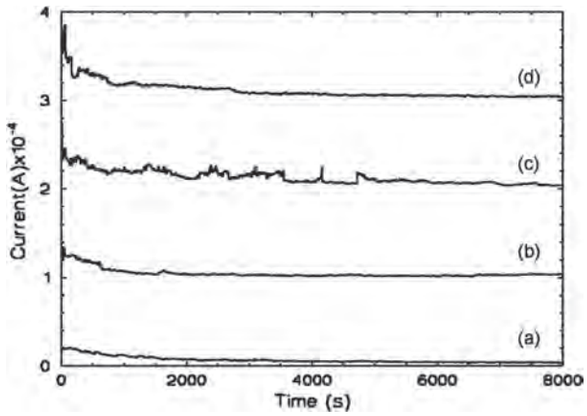

Fig. 5. Stability of the emission current over time of (a) pure ZnO (b) 3 mol% Mg-doped ZnO, (c) 5 mol% Mg-doped ZnO and (d) 10 mol% Mg-doped ZnO nanostructures.

The emission stability of pure and Mg-doped ZnO nanostructures was tested for 120 min at a fixed electric field of 1000 V and the plots for the variation of emission current with time are shown in Figure 5. The results show that the emission current stability for pure ZnO, 3 mol% Mg-doped ZnO and 10 mol% Mg-doped ZnO nanostructures were generally good even though for 5 mol% Mg-doped ZnO nanostructures, some slight fluctuations were observed. These results indicated that pure ZnO and Mg-doped ZnO nanostructures prepared by low temperature sol–gel method using *C. Aurantifolia* exhibit good emission current stability and is a good candidate for field emission device applications.

4. CONCLUSION

Pure and Mg-doped ZnO nanostructures have been synthesized using *C. Aurantifolia* fruit extract as a reducing agent by a biomolecules assisted sol–gel method. XRD results showed that pure and Mg-doped ZnO exhibits the hexagonal wurtzite structure of ZnO. The Mg atomic percentage from EDX analysis showed that the amount of Mg element in the sample increased as the dopant concentration during synthesis increases which was 0.225, 0.29 and 0.45 at.% for 3, 5, and 10 mol% Mg concentration during synthesis, respectively. Field electron emission measurements yielded a general trend of decreasing turn-on and threshold field values with increasing Mg doping level. Threshold electric field values of 6.99, 6.35, 6.07 and 5.99 V/μm were measured for pure ZnO, 3, 5, and 10 mol% Mg concentration during synthesis, respectively. Almost similar trend was observed with the turn on field values of 916, 917, 8.62 and 8.49 V/μm. The field enhancement factor, which significantly depended on the emitter geometry, showed no clear trend. Almost equal field enhancement factor values of 801, 965, 955 and 786 for pure ZnO, 3, 5 and 10 mol% Mg concentration during synthesis respectively was due to similar geometrical structure of the samples. In general, this study has demonstrated that the use *C. Aurantifolia* as a green reagent is viable for the synthesis ZnO nanostructures with good field electron emission features.

Acknowledgments: This work is funded by the University of Malaya under the UM Research Grant No. RG247-12AFR, PPP Grant No. PG068-2013A and UM.C/HIR/MOHE/SC/33.

References and Notes

1. S. J. Pearton, D. P. Norton, and K. Ip; Recent progress in processing and properties of ZnO; *Prog. Mater. Sci.* 50, 293 **(2005)**.
2. A. B. Djurišić, X. Chen, Y. H. Leung, and A. Man Ching Ng; ZnO nanostructures: Growth, properties and applications; *J. Mater. Chem.* 22, 191 **(2012)**.
3. M. Firdaus, M. Hafiz, M. Zainizan, M. Mohamed, Z. Khusaimi, and M. Rusop; Influence of various sol concentrations on stress/strain and properties of ZnO thin films synthesised by sol–gel technique; *Thin Solid Films* 527, 102 **(2013)**.
4. V. Khranovskyy, T. Ekblad, R. Yakimova, and L. Hultman; Surface morphology effects on the light-controlled wettability of ZnO nanostructures; *Appl. Surf. Sci.* 258, 8146 **(2012)**.
5. J. Chen, J. Li, J. Li, G. Xiao, and X. Yang; Large-scale syntheses of uniform ZnO nanorods and ethanol gas sensors application; *J. Alloys Compd.* 509, 740 **(2011)**.
6. L. Li, T. Zhai, Y. Bando, and D. Golberg; Recent progress of one-dimensional ZnO nanostructured solar cells; *Nano Energy* 1, 91 **(2012)**.
7. G. Zhang, Q. Zhang, Y. Pei, and L. Chen; Field emission from non-aligned zinc oxide nanostructures; *Vacuum* 77, 53 **(2004)**.
8. K. Yu, Y. Zhang, R. Xu, S. Ouyang, D. Li, and L. Luo; Efficient field emission from tetrapod-like zinc oxide nanoneedles; *Mater. Lett.* 59, 1866 **(2005)**.
9. G. Zhang, L. Wei, Y. Chen, L. Mei, and J. Jiao; Field emission property of ZnO nanoneedle arrays with different morphology; *Mater. Lett.* 96, 131 **(2013)**.
10. S. P. Dubey, M. Lahtinen, and M. Sillanpää; Tansy fruit mediated greener synthesis of silver and gold nanoparticles; *Process Biochem.* 45, 1065 **(2010)**.
11. P. S. Vankar and D. Shukla; Biosynthesis of silver nanoparticles using lemon leaves extract and its application for antimicrobial finish on fabric; *Appl. Nanosci.* 2, 163 **(2011)**.
12. N. Ahmad, S. Sharma, and R. Rai; Rapid green synthesis of silver and gold nanoparticles using peels of Punica Granatum; *Adv. Mater. Lett.* 3, 376 **(2012)**.
13. G. Sangeetha, S. Rajeshwari, and R. Venckatesh; Green synthesis of zinc oxide nanoparticles by aloe barbadensis miller leaf extract: Structure and optical properties; *Mater. Res. Bull.* 46, 2560 **(2011)**.
14. R. P. Singh; Biological approach of zinc oxide nanoparticles formation and its characterization; *Adv. Mater. Lett.* 2, 313 **(2011)**.
15. N. Ain Samat and R. Md Nor; Sol–gel synthesis of zinc oxide nanoparticles using citrus aurantifolia extracts; *Ceram. Int.* 39, S545 **(2013)**.
16. B. K. Sonawane, M. P. Bhole, and D. S. Patil; Structural, optical and electrical properties of post annealed Mg doped ZnO films for optoelectronics applications; *Opt. Quant. Electron.* 41, 17 **(2009)**.
17. J. Sengupta, A. Ahmed, and R. Labar; Structural and optical properties of post annealed Mg doped ZnO thin films deposited by the sol–gel method; *Mater. Lett.* 109, 265 **(2013)**.
18. Z. Ji, Y. Song, Y. Xiang, K. Liu, C. Wang, and Z. Ye; Characterization of MgxZn1-xO thin films prepared by sol–gel dip coating; *J. Cryst. Growth* 265, 537 **(2004)**.
19. R. H. Fowler and L. W. Nordheim; Electron emission in intense electric fields; *Proc. R. Soc. A* 119, 173 **(1928)**.

Article

20. L. L. Wang, S. D. Gong, L. H. Wu, and X. J. Li; Field emission from zinc oxide nanorod bundles grown on silicon nanoporous pillar array; *Appl. Surf. Sci.* 270, 124 **(2013)**.
21. J.-H. Lee, Y.-W. Chung, M.-H. Hon, and I.-C. Leu; Density-controlled growth and field emission property of aligned ZnO nanorod arrays; *Appl. Phys. A* 97, 403 **(2009)**.
22. R. C. Wang, C. P. Liu, J. L. Huang, S.-J. Chen, Y.-K. Tseng, and S.-C. Kung; ZnO nanopencils: Efficient field emitters; *Appl. Phys. Lett.* 87, 013110 **(2005)**.
23. H. Pan, Y. Zhu, H. Sun, Y. Feng, C.-H. Sow, and J. Lin; Electroluminescence and field emission of Mg-doped ZnO tetrapods; *Nanotechnology* 17, 5096 **(2006)**.
24. D. Pradhan, M. Kumar, Y. Ando, and K. T. Leung; Fabrication of ZnO nanospikes and nanopillars on ITO glass by templateless seed-layer-free electrodeposition and their field-emission properties; *ACS. Appl. Mat. Interface* 1, 789 **(2009)**.
25. S. S. Warule, N. S. Chaudhari, J. D. Ambekar, B. B. Kale, and M. A. More; Hierarchical nanostructured ZnO with nanorods engendered to nanopencils and pin-cushion cactus with its field emission study; *ACS. Appl. Mat. Interface* 3, 3454 **(2011)**.
26. F. J. Sheini, J. Singh, O. N. Srivasatva, D. S. Joag and M. A. More; Electrochemical synthesis of Cu/ZnO nanocomposite films and their efficient field emission behaviour; *Appl. Surf. Science* 256, 2110 **(2010)**.
27. D. Pradhan, M. Kumar, Y. Ando, and K. T. Leung; Efficient field emission from vertically grown planar ZnO nanowalls on an ITO–glass substrate; *Nanotechnology* 19, 035603 **(2008)**.
28. R. Yousefi, F. J. Sheini, M. R. Muhamad, and M. A. More; Characterization and field emission properties of ZnMgO nanowires fabricated by thermal evaporation process; *Solid State Sciences* 12, 1088 **(2010)**.
29. D. Pradhan, M. Kumar, Y. Ando, and K. T. Leung; One-dimensional and two-dimensional ZnO nanostructured materials on a plastic substrate and their field emission properties; *J. Phys. Chem. C* 112, 7093 **(2008)**.
30. F. J. Sheini, D. S. Joag, and M. A. More; Electrochemical synthesis of Sn doped ZnO nanowires on zinc foil and their field emission studies; *Thin Solid Films* 519, 184 **(2010)**.
31. F. J. Sheini, D. S. Joag, and M. A. More; Field emission studies on electrochemically synthesized ZnO nanowires; *Ultramicroscopy* 109, 418 **(2009)**.

Received: 7 August 2014. Revised/Accepted: 3 February 2015.